Structure- and composition-tunable superconductivity, band topology, and elastic response of hard binary niobium nitrides Nb_2N, Nb_4N_3 and Nb_4N_5

K. Ramesh Babu [1] and Guang-Yu Guo [1,2,*]

[1] *Department of Physics, National Taiwan University, Taipei 10617, Taiwan*

[2] *Physics Division, National Center for Theoretical Sciences, Taipei 10617, Taiwan*

(Received 28 May 2023; revised 24 July 2023; accepted 25 July 2023; published 10 August 2023)

We perform a systematic *ab initio* density functional study of the superconductivity, electronic and phononic band structures, electron-phonon coupling, and elastic constants of all four possible structures of niobium nitride β-Nb_2N as well as Nb-rich γ-Nb_4N_3 and N-rich β'-Nb_4N_5. First of all, we find that all four structures of β-Nb_2N are superconductors with superconducting transition temperatures (T_c) ranging from 0.6 to 6.1 K, depending on the structure. This explains why previous experiments reported contradicting T_c values for β-Nb_2N. Furthermore, both γ-Nb_4N_3 and β'-Nb_4N_5 are predicted to be superconductors with rather high T_c of 8.5 and 15.3 K, respectively. Second, the calculated elastic constants and phonon dispersion relations show that all the considered niobium nitride structures are mechanically and dynamically stable. Moreover, the calculated elastic moduli demonstrate that all the niobium nitrides are hard materials with bulk moduli and hardness being comparable to or larger than the well-known hard sapphire. Third, the calculated band structures reveal that the nitrides possess both type I and type II Dirac nodal points and are thus topological metals. Finally, the calculated electron-phonon coupling strength, superconductivity, and mechanical properties of the niobium nitrides are discussed in terms of their underlying electronic structures and also Debye temperatures. The present *ab initio* study thus indicates that β-Nb_2N, γ-Nb_4N_3 and β'-Nb_4N_5 are hard superconductors with nontrivial band topology and are promising materials for exploring exotic phenomena due to the interplay of hardness, superconductivity, and nontrivial band topology.

DOI: 10.1103/PhysRevB.108.064505

I. INTRODUCTION

Transition metal nitrides (TMNs) are well known for their refractory characteristics such as high mechanical strength, hardness, high melting point, excellent thermal stability, and resistance to corrosion and oxidation. These superior properties make them promising materials for many practical applications, such as wear-resistance surfaces, high pressure, and magnetic storage devices, and cutting tools [1,2]. Furthermore, TMNs are good metallic conductors and some of them exhibit superconductivity [3–8]. Interestingly, these materials were also found to possess nontrivial band topology [9–11].

Among all the TMNs, the binary niobium nitride systems are of particular interest because they exist in a variety of crystal structures with outstanding electronic and superconducting properties [12–15]. At ambient pressure, the following crystalline structures of the niobium nitrides (see Table I) are known to exist: (i) cubic α-NbN, (ii) hexagonal β-Nb_2N, (iii) tetragonal γ-Nb_4N_3, (iv) cubic δ-NbN, (v) hexagonal ε-NbN, (vi) hexagonal WC-NbN, (vii) tetragonal β'-Nb_4N_5, (viii) hexagonal δ'-NbN, and (ix) hexagonal ε'-Nb_5N_6.

One interesting feature of these nitride systems is that the Nb atoms are connected with N atoms through strong covalent bonds, thus resulting in superior mechanical properties compared to the metal carbides and oxides [16]. The superconductivity of these niobium nitrides depends on both the Nb/N ratio and the crystal structure [17] (see, e.g., Table I). For example, δ-NbN, β-Nb_2N, γ-Nb_4N_3 and β'-Nb_4N_5 are known to be superconductors while hexagonal δ'-NbN and ε'-Nb_5N_6 structures do not exhibit superconductivity down to 1.8 K [11,17]. Because of their relatively high superconducting transition temperatures and high hardness, the δ and γ phases of NbN have found applications in superconducting radio frequency circuits [18,19], Josephson junction qubits [20,21], terahertz wave detection hot-electron-bolometer [22], superconducting nanowire single-photon detectors [23] and also in the fabrication of superconducting quantum interference devices (SQUIDs) [24–26]. In addition, nitrogen rich structures β'-Nb_4N_5 and ε'-Nb_5N_6 are candidates for supercapacitor applications [27].

However, the superconductivity as well as mechanical and electronic properties of many niobium nitrides have been rather poorly understood. In particular, a wide range of superconducting transition temperatures (T_c) have been reported for the β-phase Nb_2N (β-Nb_2N) [4,5,28–30]. For example, Gavaler *et al.* reported that β-Nb_2N has a T_c value between 8.6 and 12.1 K [4]. Skokan *et al.* [5] reported that the thin films of mixed phases of cubic-NbN and hexagonal β-Nb_2N exhibit two step resistance drop at 9 K and at 2 K. Gajar *et al.* [28] reported the transformation of Nb into hexagonal β-Nb_2N which is superconducting only below 1.0 K. Very recently, Kalal *et al.* [30] claimed that the hexagonal β-Nb_2N ($P6_3/mmc$) films have the electron-phonon interaction

*gyguo@phys.ntu.edu.tw

TABLE I. Crystal structure, space group, and superconducting transition temperature T_c of some niobium nitrides.

Phase	Structure	Space group	T_c (K)
α-NbN	Cubic	$Pm\bar{3}m$	16[a]
δ-NbN	Cubic	$Fm\bar{3}m$	17.3[b]
δ'-NbN	Hexagonal	$P6_3/mmc$	<1.77[c]
ε-NbN	Hexagonal	$P6_3/mmc$	11.6[d], <1.77[c]
WC-NbN	Hexagonal	$P\bar{6}m2$	
β_1-Nb_2N	Trigonal	$P\bar{3}1m$	8.6-12.1[e], <1[f], 4.74[g]
β_2-Nb_2N	Trigonal	$P\bar{3}m1$	
β_3-Nb_2N	Hexagonal	$P6_3/mmc$	
β_4-Nb_2N	Orthorhombic	Pnnm	
γ-Nb_4N_3	Tetragonal	I4/mmm	7.8-12.2[h]
β'-Nb_4N_5	Tetragonal	I4/m	10[i], 8-16[c]

[a]References [31,32] (expt); [b]Reference [34] (expt); [c]Reference [17] (expt); [d]Reference [14] (expt); [e]Reference [4] (expt); [f]Reference [29] (expt); [g]Reference [30] (expt); [h]Reference [36] (expt); [i]Reference [37] (expt).

dominanted superconductivity with a T_c of 4.74 K. Clearly, all these experimental studies on superconductivity of β-Nb_2N contradict each other.

On the other hand, we note that at least four crystalline structures (see Table I and Fig. 1) have been reported for β-Nb_2N [33,35,38–42]. Guard *et al.* [33] reported that β-Nb_2N adopts a W_2C type structure with space group $P\bar{3}m1$. However, Christensen [35] reported that β-Nb_2N has a ε-Fe_2N type structure with space group $P\bar{3}1m$. Besides, β-Nb_2N also exists in $P6_3/mmc$ space group [42]. Recent *ab initio* random structure search also predicted that β-Nb_2N can exist in an orthorhombic structure with Pnnm space group [41]. Unfortunately, unlike niobium nitrides with other Nb/N ratios such as NbN where one structure is labeled as one phase (Table I), all the structures of Nb_2N have been labeled as the β-Nb_2N. It is well known that the superconductivity and physical properties of a solid are determined by its crystal structure, as we have recently demonstrated for NbN [11]. Consequently, we believe that the contradicting superconducting properties reported for β-Nb_2N are caused by the fact that it has several different structures, as for NbN (Table I). In this work, therefore, we perform a systematic *ab initio* study of the superconducting and also other physical properties of β-Nb_2N in all the four possible structures. Furthermore, to study how the superconductivity depends on the Nb/N ratio, we also consider Nb-rich γ-Nb_4N_3 and N-rich β'-Nb_4N_5. Both γ-Nb_4N_3 and β'-Nb_4N_5 crystallize in the tetragonal NaCl-type δ-NbN structure, respectively, by removal of half of either nitrogen or niobium atoms in alternating planes along the c axis [32]. They are also superconductors with quite high T_c values (7.8 $\sim$ 16.0 K) [17,36,37].

Materials that exhibit both superconductivity and nontrivial band topology are excellent candidates to study the fascinating phenomena such as topological superconductivity and Majorana Fermions [43]. In recent years, there is indeed a growing interest in the search for materials where superconductivty coexists with nontrivial band topology [44,45]. In the binary Nb-N systems, the electronic structure [46–49], mechanical [13,50], phonon and superconducting properties [51,52] of niobium mononitride (Nb/N = 1) have recently been extensively studied, and as a result, Dirac and Weyl nodal points have been predicted in several structures of NbN such as cubic δ-NbN, hexagonal ε-NbN, δ'-NbN, and WC-NbN by the *ab initio* calculations [9–11]. However, for either Nb-rich or N-rich niobium nitrides (i.e., niobium nitrides with Nb/N

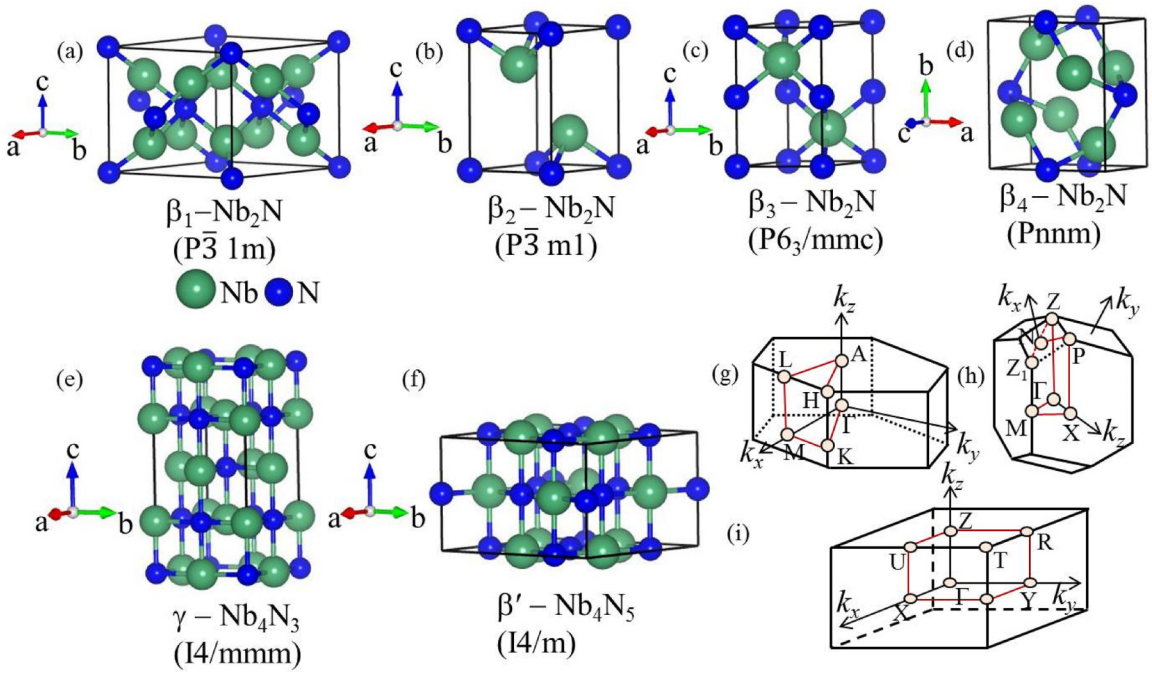

FIG. 1. Crystal structures of (a) β_1-Nb_2N, (b) β_2-Nb_2N, (c) β_3-Nb_2N, (d) β_4-Nb_2N, (e) γ-Nb_4N_3 and (f) β'-Nb_4N_5. The hexagonal Brillouin zone (BZ) of β_1-Nb_2N, β_2-Nb_2N and β_3-Nb_2N is illustrated in (g), the tetragonal BZ of γ-Nb_4N_3 and β'-Nb_4N_5 is shown in (h), and the orthorhombic BZ of β_4-Nb_2N is plotted in (i).

ratios different from 1), no theoretical studies on the band topology and superconductivity have been reported. Finally, the mechanical properties of either Nb-rich or N-rich niobium nitrides have been much less investigated and consequently remain poorly understood. This would certainly hinder their technological applications as hard superconductors. The rest of this paper is organized as follows. In Sec. II, we introduce the crystal structures of the considered nitrides, theory of superconductivity, *ab initio* calculation methods and computational details used in the present study. In Sec. III, the calculated physical properties of the niobium nitrides are presented. In particular, the theoretical elastic constants, moduli and hardness of the nitrides are reported in Sec. III A. In Sec. III B, the calculated electronic band structures are presented and Dirac nodal points are identified. In Sec. III C, the calculated phonon dispersion relations as well as the contributions from the lattice vibrations and conduction electrons to the specific heat and Debye temperatures are presented. Finally, the calculated electron-phonon coupling strengths and estimated superconducting transition temperatures are reported in Sec. III D. In Sec. IV, we summarize the conclusions drawn from this work.

II. CRYSTAL STRUCTURES AND COMPUTATIONAL METHODS

The crystal structures and the corresponding Brillouin zones of all the considered niobium nitrides are shown in Fig. 1. Four crystalline structures have been reported for β-Nb_2N, namely, trigonal $P\bar{3}1m$ (No. 162) [35] (β_1-Nb_2N) and $P\bar{3}m1$ (No. 164) [33] (β_2-Nb_2N), hexagonal $P6_3mmc$ (No. 194) [42] (β_3-Nb_2N) and orthorhombic Pnnm (No. 58) [41] (β_4-Nb_2N). The crystal structure of β_1-Nb_2N contains three formula units (f.u.) per unit cell [35]. Nb occupies the Wyckoff site 6*k* ($\frac{1}{3}$, 0, $\frac{1}{4}$), N is at 1*a* (0, 0, 0) and 2*d* ($\frac{1}{3}$, $\frac{2}{3}$, $\frac{1}{2}$). In β_2-Nb_2N, Nb is at 2*c* ($\frac{1}{3}$, $\frac{2}{3}$, $\frac{1}{4}$) and N at 2*a* (0, 0, 0) whereas in β_3-Nb_2N, Nb occupies 2*c* ($\frac{1}{3}$, $\frac{2}{3}$, $\frac{1}{4}$) and N is at 2*a* (0, 0, 0). The crystal structure of β_4-Nb_2N has two f.u. per unit cell [41]. Nb occupies 4*g* (0.2572, 0.3390, 0) and N 2*d* ($\frac{1}{2}$, 0, 0). Both γ-Nb_4N_3 and β'-Nb_4N_5 crystallize in the tetragonal structure with space group I4/mmm (No. 139) [53] and I4/m (No. 7) [54], respectively. The unit cell of γ-Nb_4N_3 contains two f.u. with Nb at 4*c* (0, $\frac{1}{2}$, 0) and 4*e* (0, 0, 0.2521) and N atoms at 2*a* (0, 0, 0) and 4*d* (0, $\frac{1}{2}$, $\frac{1}{4}$). The unit cell of β'-Nb_4N_5 has two f.u. with Nb at 8*h* (0.4, 0.2, 0) and N at 2*b* (0, 0, $\frac{1}{2}$) and 8*h* (0.1, 0.3, 0). It is worth to mention that all the crystal structures possess inversion ($\mathcal{P}$) symmetry.

The *ab initio* structural optimizations, elastic constants, electronic band structures and density of states (DOS) calculations are based on density functional theory (DFT) with the generalized gradient approximation (GGA) [55]. The calculations are performed by using the accurate projector-augmented wave method [56–58], as implemented in the Vienna *Ab initio* Simulation Package (VASP). For the Brillouin zone (BZ) integration, the tetrahedron method is used with Γ-centered *k*-point meshes of 8 × 8 × 10, 8 × 8 × 6, 8 × 8 × 6, 8 × 6 × 10, 8 × 8 × 4 and 8 × 8 × 10, respectively, for β_1-Nb_2N, β_2-Nb_2N, β_3-Nb_2N, β_4-Nb_2N, γ-Nb_4N_3, and β'-Nb_4N_5. A large plane-wave cut-off energy of 500 eV is used throughout. The DOS are calculated by using denser *k*-point meshes of 16 × 16 × 20 for β_1-Nb_2N, 16 × 16 × 12 for β_2-Nb_2N and β_3-Nb_2N, and 16 × 12 × 20 for β_4-Nb_2N, 16 × 16 × 8 for γ-Nb_4N_3 and 16 × 16 × 20 for β' - Nb_4N_5. In the crystal structure optimizations, the structures are relaxed until the atomic forces are less than 0.0001 eV/Å. A small total energy convergence criterion of 10^{-8} eV is used for all the calculations. The calculated lattice constants and total energies for all the considered structures are listed in Table II. We notice that the calculated lattice constants of all the structures are in good accord with the available experiment data [33,35,41,42,53,54] and previous theoretical calculations based on GGA. [38–40] Among the four structures of β-Nb_2N, β_1-Nb_2N is found to be the ground state structure with β_4-Nb_2N, β_2-Nb_2N, β_3-Nb_2N structures being, respectively, 0.062 eV/f.u., 0.305 eV/f.u. and 0.381 eV/f.u. higher in total energy.

TABLE II. Theoretical lattice constants ($a, b, c, c/a$), volume (V) and total energy (E_t) of all the studied niobium nitrides, compared with the available experimental data (Expt).

Phase	a (Å)	b (Å)	c (Å)	c/a	V (Å^3/at)	E_t (eV/at)
β_1-Nb_2N	5.341		5.009	0.937	13.75	−10.3743
Expt[a]	5.267		4.987	0.946		
β_2-Nb_2N	3.157		4.858	1.538	13.98	−10.2725
Expt[b]	3.058		4.961	1.622		
β_3-Nb_2N	2.999		5.605	1.868	14.56	−10.2470
Expt[c]	3.055		4.994	1.634		
β_4-Nb_2N	4.931	5.455	3.066	0.562	13.75	−10.3536
γ-Nb_4N_3	4.427		8.707	1.966	12.19	−10.2478
Expt[d]	4.382		8.632	1.969		
β'-Nb_4N_5	6.933		4.324	0.624	11.55	−10.0132
Expt[e]	6.873		4.298	0.625		

[a]References [35] (expt); [b]Reference [33] (expt); [c]Reference [42] (expt); [d]Reference [53] (expt); [e]Reference [54] (expt).

The elastic constants of the niobium nitrides are calculated by using the linear-response stress-strain method, as implemented in the VASP code [59]. Under a small strain (ε_{kl}), according to Hooke's law, the corresponding stress (σ_{ij}) can be written as $\sigma_{ij} = C_{ijkl}\varepsilon_{kl}$, where C_{ijkl} is the elastic stiffness tensor that consists of the elastic constants of the crystal. Here, for each stress, we perform the self-consistent total energy calculations by applying two strains of −1.5% and +1.5% [60,61]. The total number of elastic constants depends on the crystal symmetry. The calculated nonzero elastic constants for all the considered structures are listed in Table III. For the hexagonal and trigonal crystals, the bulk modulus B and shear modulus G are given by $B = \frac{2}{9}(C_{11} + C_{12} + 2C_{13} + \frac{1}{2}C_{33})$ and $G = \frac{1}{30}(12C_{44} + 7C_{11} - 5C_{12} + 2C_{33} - 4C_{13})$. For the tetragonal structures, $B = \frac{1}{9}\{2(C_{11} + C_{12}) + C_{33} + 4C_{13}\}$ and $G = \frac{1}{30}\{4C_{11} - 2C_{12} - 4C_{13} + 2C_{33} + 12C_{44} + 6C_{66}\}$. In the orthorhombic crystals, $B = \frac{1}{9}\{C_{11} + C_{22} + C_{33} + 2C_{12} + 2C_{13} + 2C_{23}\}$ and $G = \frac{1}{15}\{C_{11} + C_{22} + C_{33} - (C_{12} + C_{13} + C_{23})\} + \frac{3}{15}\{C_{44} + C_{55} + C_{66}\}$. The Young's modulus Y and Poisson's ratio are related to B and G by $Y = 9BG/(3B + G)$ and $\nu = (3B - 2G)/2(3B + G)$. The hardness H can be estimated by $H = 0.1769G - 2.899$. [62] From the calcu-

TABLE III. Calculated elastic constants (C_{ij}), bulk modulus (B), shear modulus (G), Young's modulus (Y), hardness (H), Poisson's ratio (ν) and B/G ratio of all the considered niobium nitrides. For comparison, the previous theoretical elastic constants of cubic δ-NbN [11] and the experimental elastic constants of the hard sapphire (α-Al_2O_3) [69,70] are also listed. Also listed are the experimental H values for β_3-Nb_2N [74,75]. The quantities C_{ij}, B, G, Y, and H are in units of GPa. The average longitudinal, transverse and average elastic wave velocities $\bar{\upsilon}_l$, $\bar{\upsilon}_t$ and $\bar{\upsilon}_m$, Debye temperature (Θ_D^e) estimated from the calculated elastic constants are also listed.

	β_1-Nb_2N	β_2-Nb_2N	β_3-Nb_2N	β_4-Nb_2N	γ-Nb_4N_3	β'-Nb_4N_5	δ-NbN[a]	α-Al_2O_3
C_{11}	417	402	555	399	597	508	692 (608[b])	497[c]
C_{12}	167	102	229	177	89	133	145 (134[b])	163[c]
C_{13}	184	173	168	181	187	134		116[c]
C_{14}	0	0						22[c]
C_{16}						0		
C_{23}				158				
C_{22}				420				
C_{33}	421	386	619	406	392	643		501[c]
C_{44}	125	150	163	140	107	154	65 (117[b])	147[c]
C_{55}				126				
C_{66}				116	91	125		
B	258	232	318	257	280	273	327 (292[b])	246[d]
G	123	140	175	124	136	170	148 (165[b])	162[d]
Y	318	348	443	319	351	422	385	
H	18.8	21.9	28.1 (35[e], 30.9[f])	19.1	21.2	27.2	23	22[d]
ν	0.29	0.25	0.27	0.28	0.29	0.24		
B/G	2.10	1.66	1.82	2.07	2.06	1.61		
$\bar{\upsilon}_l$	7.24	7.28	8.24	3.93	7.57	8.42		
$\bar{\upsilon}_t$	3.91	4.21	4.64	7.92	4.11	4.91		
$\bar{\upsilon}_m$	4.37	4.67	5.16	4.38	4.59	5.45		
Θ_D^e	543	545	578	630	594	718	637	

[a]Reference [11] (*ab initio* calculation); [b]Reference [7] (expt); [c]Reference [69] (expt); [d]Reference [70] (expt); [e]Reference [74] (expt); [f]Reference [75] (expt).

lated elastic constants, the Debye temperature (Θ_D^e) can be estimated by

$$\Theta_D^e = \frac{h}{k_B}\left[\frac{3n}{4\pi}\left(\frac{N_A\rho}{M}\right)\right]^{1/3}\bar{\upsilon}_m, \tag{1}$$

where h is Planck's constant, k_B is Boltzmann's constant, N_A is Avogadro's number, ρ is the density, M is the molecular weight, and n is the number of atoms per formula unit. The average sound velocity ($\bar{\upsilon}_m$) of a polycrystalline material is approximately given by $\bar{\upsilon}_m = [\frac{1}{3}(\frac{2}{\bar{\upsilon}_t^3} + \frac{1}{\bar{\upsilon}_l^3})]^{-1/3}$ where $\bar{\upsilon}_t$ and $\bar{\upsilon}_l$ are the average transverse and longitudinal elastic wave velocities, respectively, and are related to polycrystalline bulk modulus B and shear modulus G via $\bar{\upsilon}_l = (\frac{B+4G/3}{\rho})^{1/2}$ and $\bar{\upsilon}_t = (\frac{G}{\rho})^{1/2}$, respectively. The calculated Θ_D^e, $\bar{\upsilon}_t$, $\bar{\upsilon}_l$ and $\bar{\upsilon}_m$ are listed in Table III.

For superconductors with the dominant electron-phonon interaction, the superconducting properties can be analyzed through calculating the Eliashberg spectral function $\alpha^2F(\omega)$. Hence, we calculate the phonon dispersion relations, phonon DOS and electron-phonon interactions using the *ab initio* density functional perturbation theory (DFPT), [63] as implemented in the QUANTUM ESPRESSO code. [64] The calculations are performed using the scalar-relativistic optimized norm-conserving Vanderbilt pseudopotentials [65,66], *i. e.*, the spin-orbit coupling (SOC) is not included in these calculations. The plane wave cut-off energy is set to 42 Ry and the electronic charge density is expanded up to 168 Ry. A Gaussian broadening of 0.02 Ry is used for all the calculations. All the phonon and electron-phonon coupling calculations are perfomed with a q-grids of $4\times4\times5$, $4\times4\times3$, $4\times4\times3$, $4\times3\times5$, $4\times4\times2$, and $3\times3\times4$ for β_1-Nb_2N, β_2-Nb_2N, β_3-Nb_2N, β_4-Nb_2N, γ-Nb_4N_3, and β'-Nb_4N_5, respectively.

The strength of the electron-phonon coupling in a crystal is measured by the electron-phonon coupling constant (λ), which can be extracted from the Eliashberg spectral function [$\alpha^2F(\omega)$] via the Allen-Dynes formula [67,68]

$$\lambda = 2\int \frac{\alpha^2F(\omega)}{\omega}d\omega. \tag{2}$$

The Eliashberg spectral function is given by

$$\alpha^2F(\omega) = \frac{1}{2\pi N(E_F)}\sum_{qj}\frac{\gamma_{qj}}{\omega_{qj}}\delta(\hbar\omega - \hbar\omega_{qj}), \tag{3}$$

where $N(E_F)$ is the electronic DOS at the Fermi level (E_F), γ_{qj} is the phonon linewidth due to electron-phonon scattering, ω_{qj} is the phonon frequency of branch index j at wave vector q. Using the calculated λ, one can estimate the superconducting transition temperature T_c via McMillan-Allen-Dynes formula [67,68]

$$T_c = \frac{\omega_{log}}{1.2}\exp\left[\frac{-1.04(1+\lambda)}{\lambda - \mu^*(1+0.62\lambda)}\right], \tag{4}$$

where ω_{log} is logarithmically averaged phonon frequency and μ^* is the averaged screened electron-electron interaction.

III. RESULTS AND DISCUSSION

A. Mechanical properties

Elastic constants of a solid provide insight into mechanical stability and bonding characteristics of the material. In Table III, we list the calculated elastic constants of all the considered niobium nitrides along with the reported values of well-known hard material sapphire (α-Al_2O_3, space group R$\bar{3}$c) [69,70]. Table III shows that all the elastic constants are positive and for each considered structure, satisfy the necessary and sufficient elastic stability conditions [71,72]. Therefore, all the considered nitride structures should be elastically stable [71,72]. Table III also shows that for β_1-Nb_2N, β_3-Nb_2N, β_4-Nb_2N and β'-Nb_4N_5, C_{33} is larger than C_{11}, indicating that the materials are harder to compress along the c axis while it is softer for both β_2-Nb_2N and γ-Nb_4N_3. The calculated elastic moduli suggest that all the nitrides are hard materials. In particular, the calculated bulk modulus (B) of the niobium nitrides is either comparable to or larger than that of hard sapphire [70]. For example, for β_3-Nb_2N, the calculated B value is about 30% larger than the corresponding value of sapphire [70]. Interestingly, when compared to the niobium mononitride structures [11], e.g., δ-NbN ($B = 327$ GPa), both Nb-rich β-Nb_2N, and γ-Nb_4N_3 as well as N-rich β'-Nb_4N_5 possess up to about 20% lower B values. This indicates that both Nb-rich and N-rich niobium nitrides are softer materials compared to the niobium mononitride. Furthermore, the B of all the nitride structures is almost twice that of the shear modulus G, suggesting that G is the limiting parameter for the mechanical stability.

Young's modulus (Y) of a solid is the ratio of linear stress to strain and tells us about the stiffness of the material. The calculated Y of β_3-Nb_2N and β'-Nb_4N_5 is about 25% larger than that of the other nitrides, indicating their higher stiffness. According to Pugh's criteria [73], the value of B/G greater than (less than) 1.75 would inidcate ductile (brittle) character of the material. Table III thus shows that β_2-Nb_2N ($B/G = 1.66$) and β'-Nb_4N_5 ($B/G = 1.61$) are brittle materials while the rest ($B/G > 1.75$) are ductile materials. In particular, β_1-Nb_2N ($B/G = 2.10$) is more ductile than all the other nitrides. Poisson's ratio ν measures the stability of a material against the shear strain. Among the studied nitrides, β'-Nb_4N_5 has the smallest value ($\nu = 0.24$) indicating that it is relatively stable against shear strain compared to the other nitrides. Hardness (H) is an important elastic property which is responsible for wear behavior of materials [62]. It is clear from Table III that β_3-Nb_2N has the strongest hardness followed by β'-Nb_4N_5, β_2-Nb_2N, γ-Nb_4N_3, β_4-Nb_2N, and β_1-Nb_2N. The calculated hardness value of β_3-Nb_2N (28.1 GPa) is close to the experimental values of 35 GPa [74] and 30.9 GPa [75]. Importantly, Table III shows that the hardness H of the nitrides β_1-Nb_2N, β_2-Nb_2N, β_4-Nb_2N and γ-Nb_4N_3 is close to that of hard sapphire [70]. Both β_3-Nb_2N and β'-Nb_4N_5 are harder than sapphire because of almost 40% larger H values (Table III).

B. Band structure and Dirac nodal points

The energy bands and DOS spectra calculated without including the SOC, of all the studied structures are displayed in Figs. 2 and 3, respectively. Figures 2 and 3 show that all the considered Nb nitrides are metallic with many bands crossing E_F and also have relatively large DOS at E_F (see Table IV). Interestingly, Figs. 3(a) and 3(d) show that the DOS spectra of β_1-Nb_2N and β_4-Nb_2N are very similar, although their structures are quite different (Table I and Fig. 1). This implies that they have similar bonding characterstics. Indeed, this explain why their elastic moduli (B, G, Y and H) are very similar (see Table III). In particular, in the lower valence band region below −4.0 eV, Nb d DOS and N p DOS spectra in both cases have nearly the same magnitudes, indicating a strong covalent bonding in these two structures [Figs. 3(a) and 3(d)]. This is also the case for γ-Nb_4N_3 [Fig. 3(e)] and β'-Nb_4N_5 in the region below −2.0 eV [Fig. 3(f)]. Nevertheless, the weight of Nb d states in β_2-Nb_2N and β_3-Nb_2N becomes significantly smaller than that of N p states, indicating that the covalency in these nitrides decreases. This explains that the tetragonal γ-Nb_4N_3 and β'-Nb_4N_5 has superior mechanical properties compared to β_1-Nb_2N.

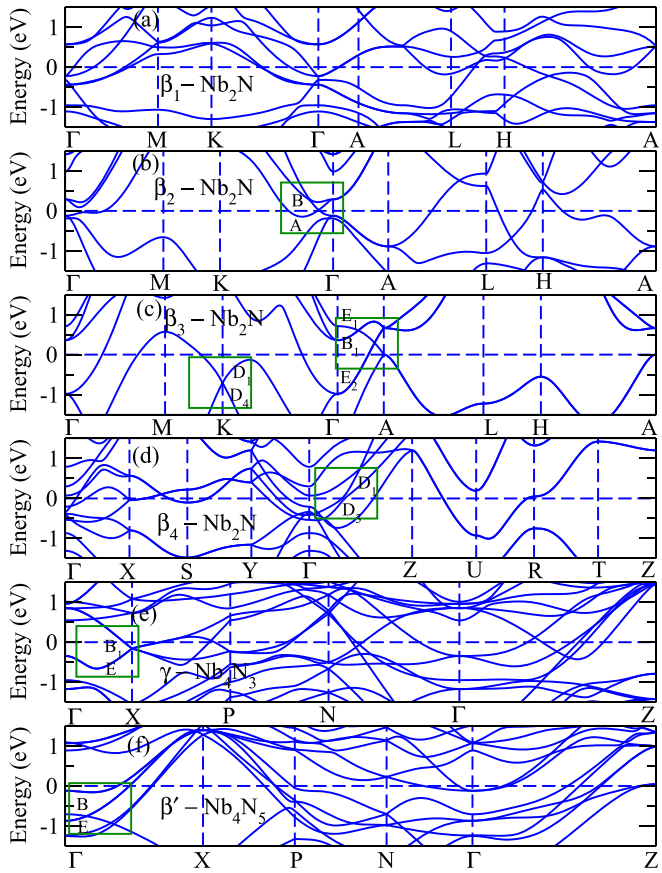

FIG. 2. Electronic band structures of (a) β_1-Nb_2N, (b) β_2-Nb_2N, (c) β_3-Nb_2N, (d) β_4-Nb_2N, (e) γ-Nb_4N_3 and (f) β'-Nb_4N_5 calculated without SOC. The green boxes indicate the band crossings with symmetries of the bands labeled.

On the other hand, Fig. 3 indicates that the upper valence bands and lower conduction bands from −4.0 to 2.0 eV of β_1-Nb_2N, β_4-Nb_2N and γ-Nb_4N_3 are Nb d dominated states. This is also the case for β'-Nb_4N_5 from −2.0 to 2.0 eV (see Fig. 3). Thus, the Nb d states are important for governing the superconducting and other transport properties of these

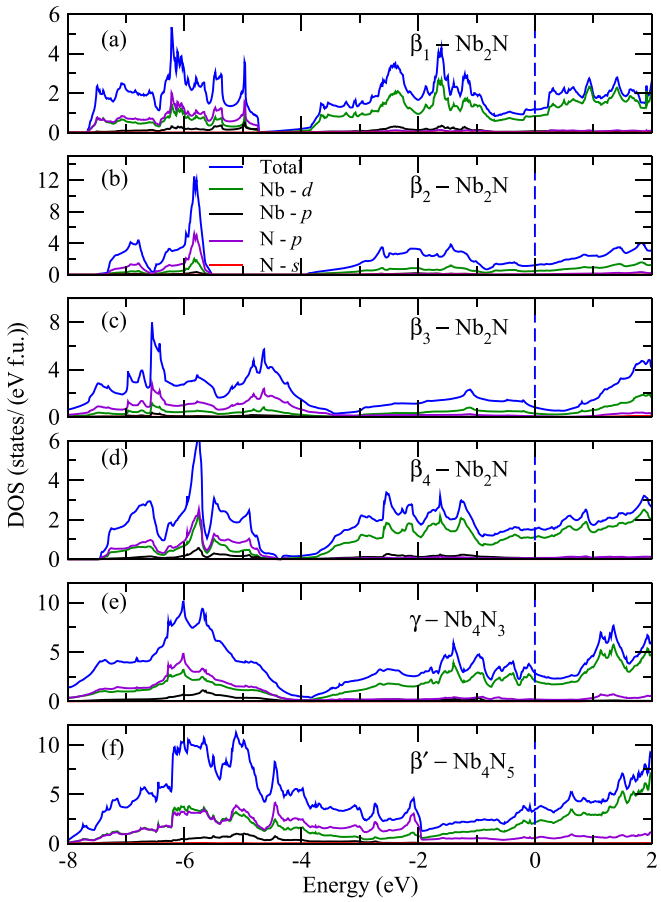

FIG. 3. Total and orbital-decomposed density of states (DOS) of (a) β_1-Nb_2N, (b) β_2-Nb_2N, (c) β_3-Nb_2N, (d) β_4-Nb_2N, (e) γ-Nb_4N_3, and (f) β'-Nb_4N_5.

nitrides. Furthermore, for β_1-Nb_2N, β_2-Nb_2N, and β_4-Nb_2N, the DOS in the vicinity of the E_F is nearly constant and takes value of 0.585 states/eV/Nb, 0.705 states/eV/Nb and 0.755 states/eV/Nb at E_F, respectively (see Fig. 3 and Table IV). In contrast, in β_3-Nb_2N [Fig. 3(c)], γ-Nb_4N_3 [Fig. 3(e)] and β'-Nb_4N_5 [Fig. 3(f)], the DOS monotonically decreases with energy and at E_F has the value of 0.610 states/eV/Nb, 0.698 states/eV/Nb, and 0.813 states/eV/Nb, respectively.

Interestingly, when the SOC is neglected, the band structure exhibits symmetry protected band crossings in the vicinity of the Fermi level along k-paths K-Γ, Γ-A and Γ-Z for β_2-Nb_2N, β_3-Nb_2N, and β_4-Nb_2N, respectively (see Fig. 2). Such band crossings also occur along Γ-X for γ-Nb_4N_3 and β'-Nb_4N_5. For β_4-Nb_2N, k-path Γ-Z belongs to the C_{2v} point group and the bands have two different irreducible representations (IRs) D_1 and D_3. In β_3-Nb_2N, Γ-A line has the C_{6v} point group symmetry and there exist two band crossings at 1.0 eV below the E_F [Fig. 2(d)]. At about 0.2 eV above the E_F, the band crossing is between a nondegenerate band with IR B_1 and a doubly degenerate band with IR E_2. The other band crossing at $\sim$ 0.6 eV involves two different bands with IRs B_1 and E_1, respectively. These two band crossings are protected by the C_{3z} rotational symmetry. Another symmetry protected band crossing with IRs D_1 (A_1) and D_4 (B_2) is visible at the high symmetry k-point K which belongs to the C_{2v} point group. Further, the band structure of β_2-Nb_2N shows a band crossing along K-Γ between the bands with different IRs A and B, which belong to the C_2 point group symmetry and hence are forbidden to mix. For tetragonal γ-Nb_4N_3, the linear band crossing between IRs B_1 and E is located along the Γ-X direction and it is protected by the C_{4v} point group symmetry. In β'-Nb_4N_5, the bands with IRs B and E cross each other along the Γ-X path and are protected by the $\mathcal{C}_4$ rotational symmetry of the C_{4v} point group.

Fully relativistic band structures of the nitrides are shown in Fig. 4. When the SOC is included, significant changes in the band structure occur. Among other things, the single point group symmetry changes to the double point group symmetry and hence the IRs of the bands change as well. Importantly, since the SOC breaks SU(2) symmetry, some band crossings

TABLE IV. Calculated electron-phonon coupling constant (λ), logarithmic average phonon frequency (ω_{log}), density of states at the Fermi level [$N(E_F)$], low temperature specific heat coefficients (γ and β), Debye temperature Θ_D [Θ_D^e] and superconducting transition temperature (T_c) of all the studied niobium nitrides. The smearing parameter (σ) used is 0.02 Ry. The screened Coulomb interaction μ^* is set to 0.10. Available experimental T_c values are also listed for comparison.

Structure	λ	ω_{log} (K)	$N(E_F)$ (states/eV/Nb)	γ (mJ/mol-K^2)	β (mJ/mol-K^4)	Θ_D [Θ_D^e] (K)	T_c (K)
β_1-Nb_2N	0.36	285	0.585	2.75	0.460	233 [543]	0.57
Expt							8.6–12.1[a]
β_2-Nb_2N	0.57	306	0.705	3.32	0.220	298 [578]	6.12
Expt							8.6–12.1[a]
β_3-Nb_2N	0.47	398	0.610	2.87	0.163	330 [630]	3.88
Expt	0.54					320[b]	<1[c], 4.74[b]
β_4-Nb_2N	0.46	289	0.755	3.56	0.270	278 [545]	2.64
γ-Nb_4N_3	0.58	262	0.698	6.57	0.880	249 [594]	8.48
Expt							7.8–12.2[d], 8–16[e]
β'-Nb_4N_5	0.92	249	0.873	8.22	0.824	277 [718]	15.28
Expt							8–16[e], 10[f]
δ-NbN	0.98	269	0.883	2.09	0.518	196 [637]	18.3

[a]Reference [4] (expt); [b]Reference [30] (expt); [c]Reference [29] (expt); [d]Reference [36] (expt); [e]Reference [17] (expt); [f]Reference [37] (expt).

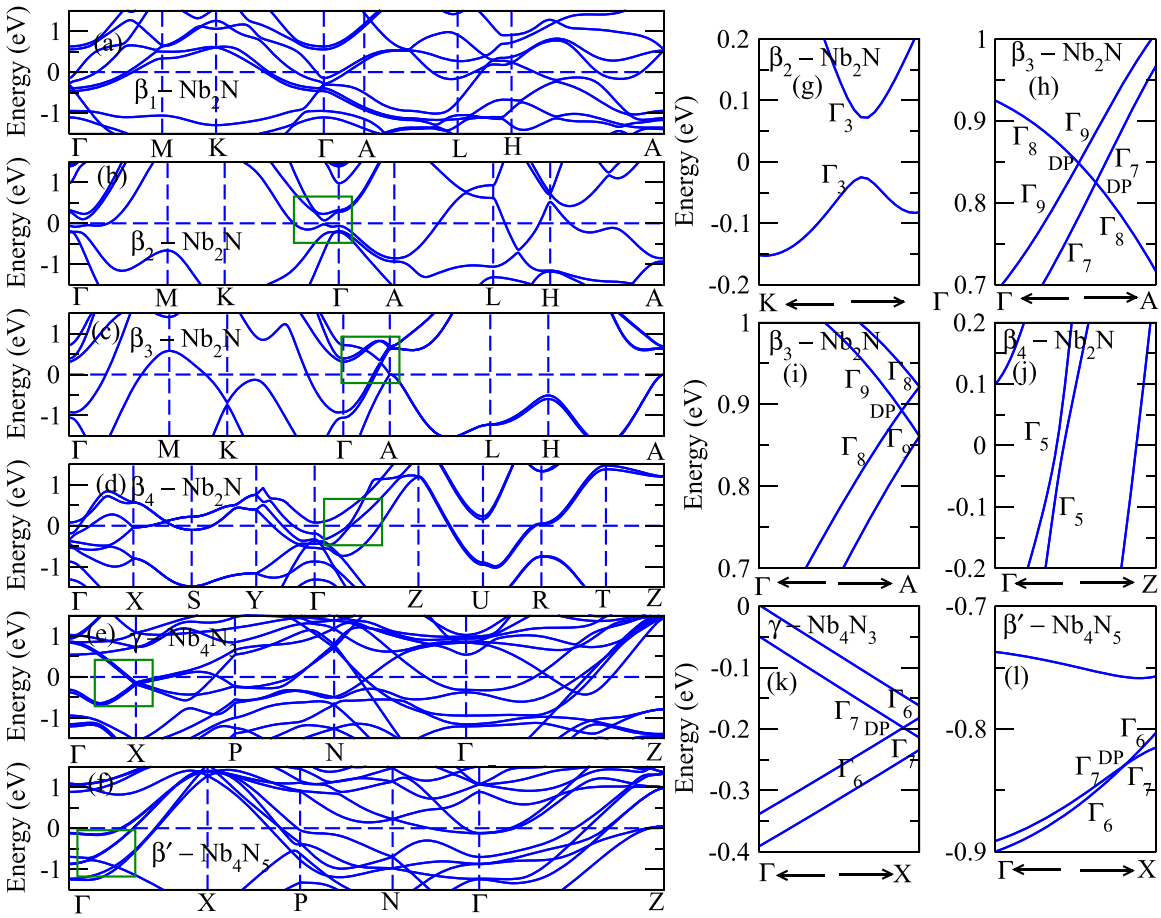

FIG. 4. Relativistic electronic band structures of (a) β_1-Nb_2N, (b) β_2-Nb_2N, (c) β_3-Nb_2N, (d) β_4-Nb_2N, (e) γ-Nb_4N_3, and (f) β'-Nb_4N_5. The right side panels (g), (h), (i)+(j), (k) and (l) correspond to the zoom-in plots of the band crossings in the green boxes in (b), (c), (d), (e) and (f), respectively. DP in (i), (j), (k), and (l) represents the Dirac point. The irreducible representations (IRs) of the band crossings in (g), (h), (i)+(j), (k), and (l) are also shown.

would become gapped. For example, the IRs D_1 and D_3 of the bands crossing along Γ-Z in β_4-Nb_2N as well as the IRs A and B of the bands crossing along Γ-K direction for β_2-Nb_2N now become Γ_5 [Figs. 4(d) and 4(j)] and Γ_3 [Figs. 4(b) and 4(g)], respectively. Both band crossings are now gapped [see Figs. 4(g) and 4(j)]. The band crossing at the K point in β_3-Nb_2N is now represented by Γ_5 (D_5) [Fig. 4(c)] and it is gapped by ∼0.05 eV. Interestingly, Fig. 4(g) shows that in β_2-Nb_2N, the Fermi level falls within the gap opened by the SOC at the band crossing. As a result, β_2-Nb_2N could exhibit large spin Hall effect due to large spin Berry curvatures induced by such SOC-gap opening [76–78], and thus might have promising applications in spintronics.

Remarkably, several band crossings remain intact after SOC is turned-on. These survived band crossings include that along the Γ-A line in hexagonal β_3-Nb_2N [Fig. 4(c)], Γ-X line in tetragonal γ-Nb_4N_3 [Fig. 4(e)] and β'-Nb_4N_5 [Fig. 4(f)]. The two band crossings along the Γ-A line in β_3-Nb_2N previously between the bands with IRs B_1 and E_2, B_1 and E_1, are now transformed from B_1 to Γ_7, E_1 and E_2 to Γ_8 and Γ_9 [Figs. 4(h) and 4(i)]. Consequently, there are now three band crossings which are protected by the mirror plane and $\mathcal{C}_{3z}$ rotational symmetry. The band crossings in γ-Nb_4N_3 along Γ-X are represented by Γ_6 and Γ_7 [Figs. 4(e) and 4(k)] and are protected by the $\mathcal{C}_4$ rotational symmetry. Furthermore, the band crossings along Γ-X in β'-Nb_4N_5 belong to the IRs Γ_6 and Γ_7 [Figs. 4(f) and 4(l)] and protected by the $\mathcal{C}_4$ symmetry. All the other band crossings become gapped out when SOC is included. Overall, there exist ungapped band crossings in the relativistic band structures along Γ-A for β_3-Nb_2N [Figs. 4(c), 4(h) and 4(i)] and along Γ-X for both γ-Nb_4N_3 [Figs. 4(e) and 4(k)] and β'-Nb_4N_5 [Figs. 4(f) and 4(l)]. This demonstrates that Nb-rich β_3-Nb_2N, γ-Nb_4N_3, and N-rich β'-Nb_4N_5 are topological metals. Importantly, all these three structures have both time-reversal ($\mathcal{T}$) symmetry and inversion ($\mathcal{P}$) symmetry and hence each energy band is twofold degenerate. Therefore, the band crossings are fourfold Dirac points (DP). In particular, the DPs in Nb-rich β_3-Nb_2N and γ-Nb_4N_3 are conventional type I whereas in N-rich β'-Nb_4N_5, the DPs are of type II because the slopes of the two crossing bands have the same sign. Finally, Fig. 4(k) shows that in γ-Nb_4N_3, the band crossing is just 0.2 eV below the Fermi level, which could be easily reached by a small amount of hole-doping via, e.g., substituting some Nb atoms with Zr atoms.

C. Lattice dynamics and specific heat

The calculated phonon dispersion relations and phonon DOS spectra of all the considered niobium nitrides are

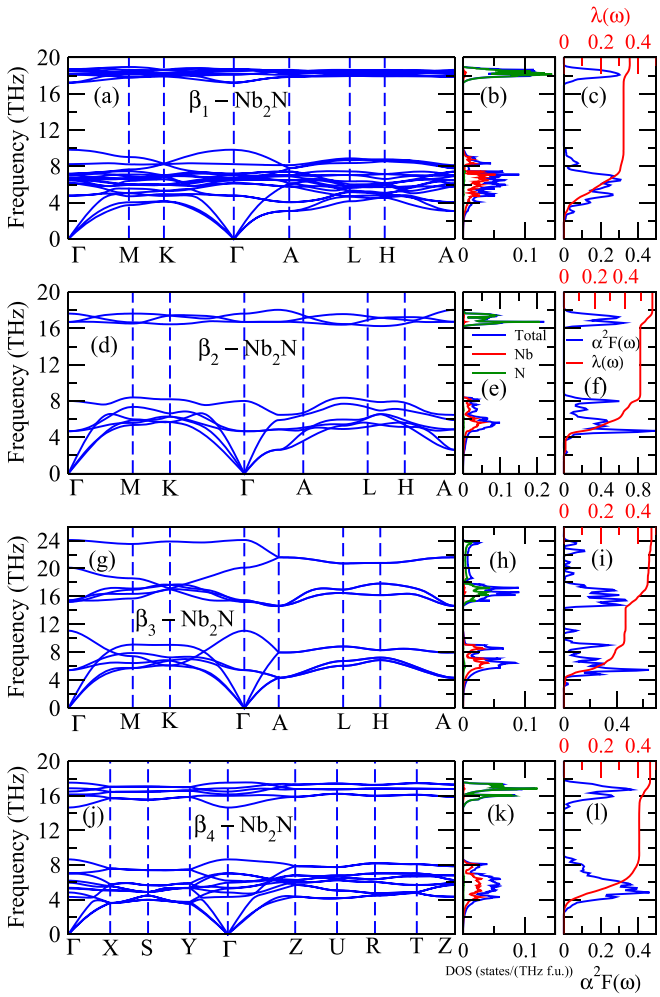

FIG. 5. Phonon dispersion relations, phonon DOS, Eliashberg function $\alpha^2F(\omega)$ and $\lambda(\omega)$ of β_1-Nb_2N (a)–(c), β_2-Nb_2N (d)–(f), β_3-Nb_2N (g)–(i) and β_4-Nb_2N (j)–(l).

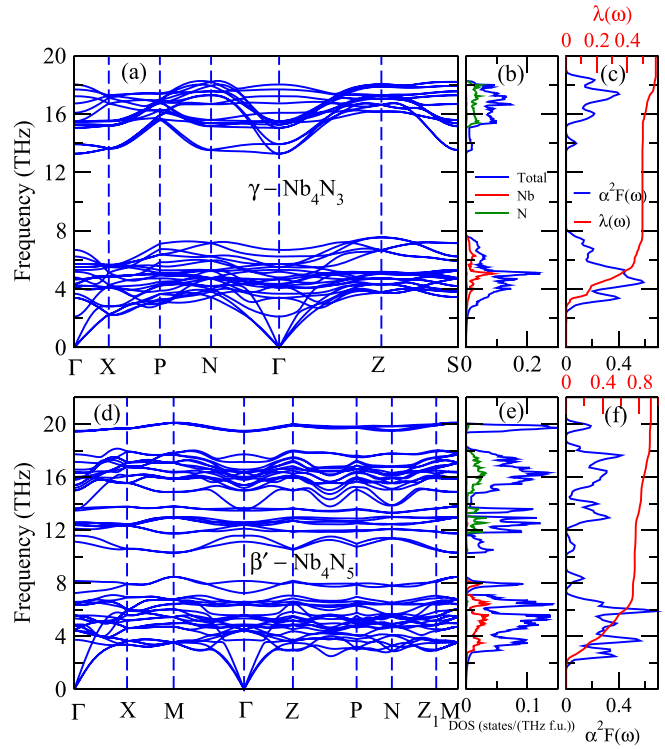

FIG. 6. Phonon dispersion, phonon DOS, Eliashberg function $\alpha^2F(\omega)$ and $\lambda(\omega)$ of γ-Nb_4N_3 (a)–(c) and β'-Nb_4N_5 (d)–(f).

presented in Figs. 5 and 6. First, the absence of any imaginary frequencies in the phonon dispersion relations throughout the Brillouin zone shows the dynamical stability of the niobium nitride structures, even although some of them are not the ground state structures (Table II). There are no experimental data available on the phonon dispersion relations of the considered nitrides. Second, Figs. 5 and 6 indicate that the phonon dispersions exhibit a large gap between the Nb atom dominated low-energy modes and the N atom dominated high-energy modes. This is due to the large mass difference between the light N atoms and the heavier Nb atoms. Furthermore, a significant mixing of low-lying optical modes with the acoustic modes exists, suggesting that a strong bonding between the Nb and the N atoms.

The calculated phonon DOS is used to obtain the specific heat $[C_v(T)]$ with the formula [79]

$$C_v(T) = \gamma T + \int d\omega \frac{(\hbar\omega)^2}{(k_BT)^2} \frac{g(\omega)e^{\hbar\omega/k_BT}}{(e^{(\hbar\omega/k_BT)}-1)^2} = \gamma T + \beta T^3, \tag{5}$$

where the first and second terms are, respectively, the electron and phonon contributions to the specific heat. Here $\gamma = \frac{\pi^2}{3}k_B^2N(E_F)$ is Sommerfeld coefficient [80] which is proportional to the electron DOS at E_F, k_B is Boltzmann constant and $g(\omega)$ is phonon DOS. To estimate the coefficient β of the phonon contribution at low temperatures, we first calculate $C_v(T)$ as a function of temperature between 4 and 9 K. The calculated $C_v(T)$ is then plotted as $\frac{C_v}{T}$ vs T^2 and fitted to $\frac{C_v}{T} = \gamma + \beta T^2$. The resulting values of γ and β for the considered niobium nitrides are listed in Table IV. Since γ is proportional to $N(E_F)$, β_1-Nb_2N and β'-Nb_4N_5 possess the lowest and highest values of γ among the niobium nitrides, respectively. There are no experimental γ data available to compare with. However, if we incorporate the electron-phonon coupling (λ), the electron specific heat γ takes the form of $\frac{\gamma_{exp}}{\gamma_{th}} = 1 + \lambda$. Thus, we can expect that $\frac{\gamma_{exp}}{\gamma_{th}} > 1$. Finally, the values of β are used to calculate the Debye temperature Θ_D by using the relation [79] $\Theta_D = (\frac{12\pi^4N_Ank_B}{5\beta})^{\frac{1}{3}}$, where N_A is the Avagadro's number and n is the number of atoms per formula unit. In Table IV, we list the calculated values of Θ_D for the niobium nitride structures. Among the niobium nitrides, β_3-Nb_2N possess the largest Θ_D, which is expected because of its smallest value of β. Only the experimental Θ_D value for β_4-Nb_2N has been reported, which agrees well with the calculated Θ_D value but is only half of the Θ_D^e value estimated using the calculated elastic constants (see Tables III and IV). We notice that the Θ_D obtained from the specific heat is generally about 50% smaller than that (Θ_D^e) (Table IV). This discrepancy may be due to the fact that the Θ_D calculated by fitting the low-temperature specific heat which is more appropriate for single

crystals, whereas Θ_D^e obtained from the elastic constants is more suitable for polycrystalline systems. We also note that this kind of discrepancy was reported before, e.g., for $TiSi_2$ where Θ_D^e of 788 K estimated from the elastic constants is over 50% higher than Θ_D of 510 K obtained from the specific heat measurements at low temperatures [81].

D. Electron-phonon coupling and superconductivity

We display in Figs. 5 and 6 the calculated $\alpha^2F(\omega)$ and $\lambda(\omega)$ of the studied niobium nitrides. Equation (2) indicates that $\alpha^2F(\omega)$ is essentially the phonon DOS spectrum modulated by the electron-phonon interaction matrix element γ_{qj} divided by the phonon frequency ω_{qj}. As a result, the $\alpha^2F(\omega)$ spectrum for each structure roughly follows the corresponding phonon DOS spectrum (see Figs. 5 and 6). Therefore, the contribution from the acoustic and low energy lying optical phonon bands to the $\alpha^2F(\omega)$ may become dominant. This is evident by the existence of large peaks in the $\alpha^2F(\omega)$ spectrum. Interestingly, among the β-Nb_2N structures, the magnitude of $\alpha^2F(\omega)$ is highest in the β_2-Nb_2N [Fig. 5(f)] and lowest for β_1-Nb_2N [5(c)]. For tetragonal structures, $\alpha^2F(\omega)$ of β'-Nb_4N_5 shows the larger peaks than for γ-Nb_4N_3 [Figs. 6(f) and 6(c)]. Overall, the magnitude of $\alpha^2F(\omega)$ is highest for β'-Nb_4N_5 and lowest for β_1-Nb_2N. Note that the strength of the electron-phonon coupling (λ) is given by an integral of Eliashberg function $\alpha^2F(\omega)$ divided by phonon frequency ω over the entire phonon frequency range (Eq. 1). This results in the lowest value of λ (0.36) for β_1-Nb_2N and highest λ (0.92) for β'-Nb_4N_5. In Table IV, we list the calculated λ values for all the niobium nitrides. Clearly, the λ value (0.92) of β'-Nb_4N_5 is much larger than that of γ-Nb_4N_3 (0.58), β_3-Nb_2N (0.47), β_2-Nb_2N (0.57) and β_1-Nb_2N (0.36). Furthermore, the calculated $\lambda(\omega)$ spectra displayed in Figs. 5 and 6, indicate that the Nb atoms have the dominant contribution to λ. Specifically, the contributions from the Nb atoms and N atoms to the total λ are as follows: Nb 89% and N 11% for β_1-Nb_2N, Nb 86% and N 14% for β_2-Nb_2N, Nb 68% and N 34% for β_3-Nb_2N, Nb 87% and N 13% for β_4-Nb_2N, Nb 83% and N 17% for γ-Nb_4N_3, Nb 80% and N 20% for β'-Nb_4N_5. In particular, Fig. 6(f) indicates that in β'-Nb_4N_5, the integrated $\lambda(\omega)$ already reaches to 0.75 when ω rises just above the Nb dominated phonon bands, thus resulting in the largest total λ and hence the highest T_c among the studied nitrides.

As mentioned already in Sec. I, the experimental studies [4,5,28–30] on the superconducting properties of β-Nb_2N so far have reported conflicting results. Gavaler *et al.* [4] reported the formation of hexagonal β-Nb_2N in a thin film using the x-ray diffraction data with some additional peaks which were not indexed, and also a T_c of 8.6 K in the thin films. In addition, they also reported another film which has mixed phases of hexagonal β-Nb_2N and cubic-NbN with a T_c of 12.1 K [1]. Skokan *et al.* [5] reported that the thin films of mixed phases of cubic-NbN and hexagonal β-Nb_2N exhibit two step resistance drop at 9 and at 2 K. Gajar *et al.* [28] reported the transformation of Nb into hexagonal β-Nb_2N which becomes superconducting below 1 K only. However, Kalal *et al.* [30] recently reported that the hexagonal β-Nb_2N ($P6_3/mmc$) films have rather strong electron-phonon interaction ($\lambda = 0.54$) with a T_c of 4.74 K.

As mentioned before, four crystalline structures (see Fig. 1) have been reported for the β-phase Nb_2N [33,35,41,42]. This is quite unlike other niobium nitrides with different Nb/N ratios. For example, different structures of NbN were labeled as different phases (one structure, one phase) (see Table I). Since the physical properties of a solid depend significantly on the crystalline structure, the contradicting superconductivity reported for β-Nb_2N could certainly be attributed to the fact that β-Nb_2N has several different structures. This has motivated us to carry out this *ab initio* theoretical study on the superconducting properties of β-Nb_2N in all four reported structures.

By using Allen-Dynes formula [Eq. (3)] and the calculated λ as well as the other phonon and electron parameters, we estimate the T_c values for all the considered nitrides, as listed in Table IV. First of all, we notice that the calculated T_c values for γ-Nb_4N_3 (8.48 K) and β'-Nb_4N_5 (15.3 K) agree rather well with the corresponding experimental values [17,29,36,37] (see Table IV). Second, different structures of β-Nb_2N indeed have rather different T_c values, ranging from ~0.6 to 6.1 K (Table IV). The calculated T_c of β_2-Nb_2N ($P\bar{3}m1$) (6.1 K) is larger than β_3-Nb_2N ($P6_3mmc$) (3.9 K), β_4-Nb_2N ($Pnnm$) (2.6 K) and β_1-Nb_2N ($P\bar{3}\,1m$) (0.6 K). These results clearly demonstrate that further experiments measuring the superconductivity and crystalline structure simultaneously on the same sample would be needed to clarify the current confusing experimental results for β-Nb_2N.

It is useful to find connections between the superconductivity and other physical properties of the nitrides. This could be helped by McMillan-Hopfield formula [67] $\lambda = [\frac{N(E_F)}{\langle\omega^2\rangle}]\Sigma_i(\frac{\langle I^2\rangle_i}{M_i})$ where $\langle I^2\rangle_i$ is the square of the electron-phonon coupling matrix element averaged over the Fermi surface and M_i is the atomic mass of ith atom. Also, $\langle\omega^2\rangle \approx 0.5\Theta_D^2$. Clearly, this indicates that λ and hence, T_c would depend on $N(E_F)$ and would be relatively large for the electronic bands with a high DOS near the Fermi energy. The calculated DOS spectra shown in Fig. 3, indicate that the Nb d-states dominate the DOS near E_F for all the structures, and therefore would make major contributions to the electron-phonon coupling and superconductivity. Thus, the calculated $N(E_F)$ per Nb atom for the considered nitrides are listed in Table IV. As can be seen from Table IV, for the considered nitrides, roughly, λ and T_c are larger with larger $N(E_F)$ and smaller Θ_D. For example, δ-NbN has the largest λ, T_c and $N(E_F)$ but the smallest Θ_D (Table IV).

IV. CONCLUSION

By performing systematic *ab initio* calculations based on the DFT and DFPT, we have investigated the superconductivity, electronic, and phononic band structures, electron-phonon coupling and elastic constants of all four reported structures of β-Nb_2N as well as Nb-rich γ-Nb_4N_3 and N-rich β'-Nb_4N_5. First, all four structures of β-Nb_2N are found to be superconductors with T_c ranging from 0.6 K to 6.1 K, depending on their structure (Table IV). This finding thus clarifies the long standing confusion that although Nb_2N was labeled as the

single β phase, contradicting T_c values for β-Nb_2N have been reported in previous experiments. Interestingly, γ-Nb_4N_3 and β'-Nb_4N_5 are predicted to be superconductors with rather high T_c of 8.5 K and 15.3 K, respectively. Second, all the calculated elastic constants and phonon frequencies are positive and also satisfy the necessary and sufficient elastic stability conditions [71,72], thereby showing that all the considered niobium nitride structures are mechanically and dynamically stable. This suggests that although only β_1-Nb_2N is found to be the ground state, the other three structures of β-Nb_2N could be grown in, e.g., the β-Nb_2N films. Furthermore, the calculated elastic moduli show that all the niobium nitrides are hard materials with bulk moduli and hardness being comparable to or even larger than the well-known hard sapphire. Third, the calculated electronic band structures reveal that β_3-Nb_2N, γ-Nb_4N_3 and β'-Nb_4N_5 are topological metals. Specifically, β_3-Nb_2N and γ-Nb_4N_3 possess type-I Dirac nodal points whereas β'-Nb_4N_5 has type-II Dirac points. Finally, the calculated electron-phonon coupling strength, superconductivity and mechanical property of the niobium nitrides are discussed in terms of their underlying electronic structures and also Debye temperatures. For example, that β'-Nb_4N_5 has the largest λ and highest T_c among the considered niobium nitrides, could be attributed to its largest DOS at E_F. All these interesting findings indicate that β-Nb_2N, γ-Nb_4N_3 and β'-Nb_4N_5 are hard superconductors with nontrivial band topology and are promising materials for studying fascinating phenomena arising from the interplay of hardness, superconductivity and nontrivial band topology.

ACKNOWLEDGMENTS

The authors acknowledge the support from the National Science and Technology Council and National Center for Theoretical Sciences (NCTS) in Taiwan. The authors are also grateful to the National Center for High-performance Computing (NCHC) in Taiwan for the computing time.

[1] L. E. Toth, *Transition Metal Carbides and Nitrides* (Academic, New York, 1971).

[2] A. Zerr, G. Miehe, and R. Riedel, Synthesis of cubic zirconium and hafnium nitride having Th_3P_4 structure, Nat. Mater. **2**, 185 (2003).

[3] M. W. Williams, K. M. Ralls, and M. R. Pickus, Superconductivity of cubic niobium carbonitrides, J. Phys. Chem. Solids **28**, 333 (1967).

[4] J. R. Gavaler, J. K. Hulm, M. A. Janocko, and C. K. Jones, Preparation and superconducting properties of thin films of transition metal interstetial compounds, J. Vac. Sci. Technol. **6**, 177 (1969).

[5] M. R. Skokan, E. F. Skelton, and E. Cukauskas, Superconducting properties and structural phase transformation of β-Nb_2N induced by C^+, and N^+-implantation, J. Phys. Chem. Solids **41**, 977 (1980).

[6] K. S. Keskar, T. Yamashita, and Y. Onodera, Superconducting transition temperatures of R. F. sputtered NbN films, Jpn. J. Appl. Phys. **10**, 370 (1971).

[7] X. J. Chen, V. V. Struzhkin, Z. Wu, M. Somayazulu, J. Qian, S. Kung, A. N. Christensen, Y. Zhao, R. E. Cohen, H. k. Mao, and R. J. Hemley, Hard superconducting nitrides, Proc. Natl. Acad. Sci. USA **102**, 3198 (2005).

[8] C. Wang, Y. Wang, X. Wu, X. Li, and J. Luo, The preparation and superconducting properties of Mo_2N nano films by high temperature nitriding method, Mater. Lett. **287**, 129292 (2021).

[9] Z. Zhu, G. W. Winkler, Q. Wu, J. Li, and Alexey A. Soluyanov, Triple Point Topological Metals, Phys. Rev. X **6**, 031003 (2016).

[10] G. Chang, S. Y. Xu, S. M. Huang, D. S. Sanchez, C. H. Hsu, G. Bian, Z. M. Yu, I. Belopolski, N. Alidoust, H. Zheng, T. R. Chang, H. T. Jeng, S. A. Yang, T. Neupert, H. Lin, and M. Zahid Hasan, Nexus fermions in topological symmorphic crystalline metals, Sci. Rep. **7**, 1688 (2017).

[11] K. R. Babu and G. Y. Guo, Electron-phonon coupling, superconductivity, and nontrivial band topology in NbN polytypes, Phys. Rev. B **99**, 104508 (2019).

[12] E. I. Isaev, S. I. Simak, I. A. Abrikosov, Y. K. Vekilov, M. I. Katsnelson, A. I. Lichtenstein, and B. Johansson, Phonon related properties of transition metals, their carbides, and nitrides: A first-principles study, J. Appl. Phys. **101**, 123519 (2007).

[13] V. I. Ivashchenko, P. E. A. Turchi, and E. I. Olifan, Phase stability and mechanical properties of niobium nitrides, Phys. Rev. B **82**, 054109 (2010).

[14] Y. Zou, X. Wang, T. Chen, X. Li, X. Qi, D. Welch, P. Zhu, B. Liu, T. Cui, and B. Li, Hexagonal-structured ε-NbN: Ultra-incompressibility, high shear rigidity, and a possible hard superconducting material, Sci. Rep. **5**, 10811 (2015).

[15] Y. Zou, X. Qi, Cheng Zhang, S. Ma, W. Zhang, Y. Li, T. Chen, X. Wang, Z. Chen, D. Welch, P. Zhu, B. Liu, Q. Li, T. Cui, and B. Li, Discovery of superconductivity in hard hexagonal ε-NbN, Sci. Rep. **6**, 22330 (2016).

[16] A. Miura, T. Takei, N. Kumada, S. Wada, E. Magome, C. Moriyoshi, and Y. Kuroiwa, Bonding preference of carbon, nitrogen, and oxygen in niobium-based rock-salt structures, Inorg. Chem. **52**, 9699 (2013).

[17] G. Oya and Y. Onodera, Transition temperatures and crystal structures of single-crystal and polycrystalline NbN_x films, J. App. Phys. **45**, 1389 (1974).

[18] L. Zhang, N. Yoshikawa, and M. Sugahara, Sub-micron field effect transistor using granular NbN thin films, IEEE Trans. Appl. Supercond. **3**, 1987 (1993).

[19] M. Radparvar, L. S. Yu-Jahnes, and R. T. Hunt, All niobium nitride Josephson tunnel junctions with thermally oxidized magnesium barrier, IEEE Trans. Appl. Supercond. **3**, 2050 (1993).

[20] Y. Nakamura, H. Terai, K. Inomata, T. Yamamoto, W. Qiu, and Z. Wang, Superconducting qubits consisting of epitaxially grown NbN/AlN/NbN Josephson junctions, Appl. Phys. Lett. **99**, 212502 (2011).

[21] K. Senapati, M. G. Blamire, and Z. H. Barber, Spin-filter Josephson junctions, Nat. Mater. **10**, 849 (2011).

[22] S. Guo, Q. Chen, D. Pan, Y. Wu, X. Tu, G. He, H. Han, F. Li, X. Jia, Q. Zhao, H. Zhang, X. Bei, J. Xie, L. Zhang, J. Chen, L. Kang, and P. Wu, Fabrication of superconducting niobium

nitride nanowire with high aspect ratio for X-ray photon detection, Sci. Rep. **10**, 9057 (2020).

[23] N. Cucciniello, D. Lee, H. Y. Feng, Z. Yang, H. Zeng, P. Nag, M. Zhu, and Q. Jia, Superconducting niobium nitride: A perspective from processing, microstructure, and superconducting property for single photon detectors, J. Phys.: Condens. Matter **34**, 374003 (2022).

[24] S. Kuriki, M. Matsuda, and A. Noya, DC SQUIDS made of NbN/a-Si/NbN tunnel junctions, IEEE Trans. Magnetics **23**, 1064 (1987).

[25] Q. Liu, H. Wang, Q. Zhang, J. Ren, W. Peng, and Z. Wang, All-NbN DC-SQUID magnetometer based on NbN/AlN/NbN Josephson junctions, IEEE Trans. Appl. Supercond. **27**, 1600204 (2017).

[26] Q. Zhang, H. Wang, X. Tang, W. Peng, and Z. Wang, Fabrication and characteristics of all-NbN SQUID series array, IEEE Trans. Appl. Supercond. **30**, 1600103 (2020).

[27] H. Cui, G. Zhu, X. Liu, F. Liu, Y. Xie, C. Yang, T. Lin, H. Gu, and F. Huang, Niobium nitride Nb_4N_5 as a new high-performance electrode material for supercapacitors, Adv. Sci. **2**, 1500126 (2015).

[28] B. Gajar, S. Yadav, D. Sawle, K. K. Maurya, A. Gupta, R. P. Aloysius, and S. Sahoo, Substrate mediated nitridation of niobium into superconducting β-Nb_2N thin films for phase slip study, Sci. Rep. **9**, 8811 (2019).

[29] J. G. Wright, H. G. Xing, and D. Jena, Growth windows of epitaxial NbN_x films on *c*-plane sapphire and their structural and superconducting properties, Phys. Rev. Mater. **7**, 074803 (2023).

[30] S. Kalal, A. Tayal, S. Karmakar, R. Joshi, R. Rawat, and M. Gupta, Electron–phonon interactions and superconductivity of β-Nb_2N thin films, Appl. Phys. Lett. **122**, 072602 (2023).

[31] G. Brauer, Nitrides, carbonitrides, and oxynitdrides of niobium, J. Less-Common Met. **2**, 131 (1960).

[32] G. Brauer and R. Esselborn, Nitridphasen des Niobs, Z. Anorg. Allg. Chem. **309**, 151 (1961).

[33] R. W. Guard, J. W. Savage, and D. G. Swarthout, Constitution of a portion of the niobium (columbium)-nitrogen system, Trans. AIME **239**, 643 (1967).

[34] H. J. Goldschmidt, *Interstitial Alloys* (Butterworths, London, 1967).

[35] A. N. Christensen, Preparation and crystal structure of β-Nb_2N and γ-NbN, Acta Chem. Scandinavica **30A**, 219 (1976).

[36] R. Kaiser, W. Spengler, S. Schicktanz, and C. Politis, Raman spectra and superconductivity of various phases of a high T_c superconductor: NbN, Phys. Status Solidi B **87**, 565 (1978).

[37] R. Marchand, F. Tessier, and F. J. Disalvo, New routes to transition metal nitrides: Preparation and characterization of new phases, J. Mater. Chem. **9**, 297 (1999).

[38] M. Sahnoun, J. C. Parlebas, M. Driz, and C. Daul, Structural and electronic properties of isostructural transition metal nitrides, Physica B **405**, 3822 (2010).

[39] T. Chihi, J. C. Parlebas, and M. Guemmaz, First principles study of structural, elastic, electronic and optical properties of Nb_2N and Ta_2N compounds, Phys. Status Solidi B **248**, 2787 (2011).

[40] R. Yu, Y. Jiang, and R. Zhou, First-principle studies of the stability, electronic and elastic properties of trigonal-type M_2N (M = Cr, V, Nb and Ta), Solid State Commun. **186**, 32 (2014).

[41] Z. Zhao, K. Bao, F. Tian, D. Duan, B. Liu, and T. Cui, Phase diagram, mechanical properties, and electronic structure of Nb–N compounds under pressure, Phys. Chem. Chem. Phys. **17**, 22837 (2015).

[42] N. Terao, Structure des nitrures de niobium, Jpn. J. Appl. Phys. **4**, 353 (1965).

[43] X. L. Qi and S. C. Zhang, Topological insulators and superconductors, Rev. Mod. Phys. **83**, 1057 (2011).

[44] M. A. Rampp, E. J. Konig, and J. Schmalian, Topologically Enabled Superconductivity, Phys. Rev. Lett. **129**, 077001 (2022).

[45] M. M. Sharma, P. Sharma, N. K. Karn, and V. P. S. Awana, A comprehensive review on topological superconducting materials and interfaces, Supercond. Sci. Technol. **35**, 083003 (2022).

[46] L. F. Mattheiss, Electronic band structure of niobium nitride, Phys. Rev. B **5**, 315 (1972).

[47] D. J. Chadi and M. L. Cohen, Electronic band structures and charge densities of NbC and NbN, Phys. Rev. B **10**, 496 (1974).

[48] K. Schwarz, The electronic structure of NbC and NbN, J. Phys. C **10**, 195 (1977).

[49] L. B. Litinskii, The band structure of hexagonal NbN, Solid State Commun. **71**, 299 (1989).

[50] C. Wang, W. Wen, Y. Su, L. Xu, C. Qu, Y. Zhang, L. Qiao, S. Yu, W. Zheng, and Q. Jiang, First-principles calculations on the mechanical properties of niobium nitrides, Solid State Commun. **149**, 725 (2009).

[51] B. Palanivel, G. Kalpana, and M. Rajagopalan, Electronic structure and superconductivity of NbN under high pressure, Phys. Status Solidi B **176**, 195 (1993).

[52] E. I. Isaev, R. Ahuja, S. I. Simak, A. I. Lichtenstein, Y. K. Vekilov, B. Johansson, and I. A. Abrikosov, Anomalously enhanced superconductivity and *ab initio* lattice dynamics in transition metal carbides and nitrides, Phys. Rev. B **72**, 064515 (2005).

[53] P. Villars and L. D. Calvert, *Pearson's Handbook of Crystallographic Data for Intermetallic Phases* (ASM, Materials Park, OH, 1991), Vol. 4.

[54] N. Terao, New phases of niobium nitride, J. Less-Common Met. **23**, 159 (1971).

[55] J. P. Perdew, K. Burke, and M. Ernzerhof, Generalized Gradient Approximation Made Simple, Phys. Rev. Lett. **77**, 3865 (1996).

[56] G. Kresse and J. Hafner, *Ab initio* molecular dynamics for liquid metals, Phys. Rev. B **47**, 558 (1993).

[57] P. E. Blöchl, Projector augmented-wave method, Phys. Rev. B **50**, 17953 (1994).

[58] G. Kresse and J. Furthmüller, Efficiency of *ab-initio* total energy calculations for metals and semiconductors using a plane-wave basis set Comput. Mater. Sci. **6**, 15 (1996).

[59] Y. L. Page and P. Saxe, Symmetry-general least-squares extraction of elastic data for strained materials from *ab initio* calculations of stress, Phys. Rev. B **65**, 104104 (2002).

[60] W. Y. Ching, P. Rulis, and A. Misra, *Ab initio* elastic properties and tensile strength of crystalline hydroxyapatite, Acta Biomaterialia **5**, 3067 (2009).

[61] H. Yao, L. Ouyang, and W. Y. Ching, *Ab initio* calculation of elastic constants of ceramic Crystals, J. Am. Ceram. Soc. **90**, 3194 (2007).

[62] A. Bouhemadou, D. Allali, S. Bin-Omran, E. M. A. Al Safi, R. Khenata, and Y. Al-Douri, Elastic and thermodynamic properties of the SiB_2O_4 (B = Mg, Zn and Cd) cubic spinels: An

ab initio FP-LAPW study, Mater. Sci. Semicond. Proce. **38**, 192 (2015).

[63] S. Baroni, S. de Gironcoli, A. Dal Corso, and P. Giannozzi, Phonons and related crystal properties from density-functional perturbation theory, Rev. Mod. Phys. **73**, 515 (2001).

[64] P. Giannozzi *et al.*, QUANTUM ESPRESSO: a modular and open-source software project for quantum simulations of materials, J. Phys.: Condens. Matter **21**, 395502 (2009).

[65] D. R. Hamann, Optimized norm-conserving Vanderbilt pseudopotentials, Phys. Rev. B **95**, 239906(E) (2017).

[66] J. P. Perdew, J. A. Chevary, S. H. Vosko, K. A. Jackson, M. R. Pederson, D. J. Singh, and C. Fiolhais, Atoms, molecules, solids, and surfaces: applications of the generalized gradient approximation for exchange and correlation, Phys. Rev. B **46**, 6671 (1992).

[67] W. L. McMillan, Transition temperature of strong-coupled superconductors, Phys. Rev. **167**, 331 (1968).

[68] P. B. Allen and R. C. Dynes, Superconductivity at very strong coupling, J. Phys. C **8**, L158 (1975).

[69] D. B. Hovis, A. Reddy, and A. H. Heuer, X-ray elastic constants for α-Al_2O_3, Appl. Phys. Lett. **88**, 131910 (2006).

[70] D. M. Teter, Computational alchemy: The search for new superhard materials, MRS Bulletin **23**, 22 (1998).

[71] M. Born and K. Huang, *Dynamical Theory of Crystal Lattices* (Oxford University Press, Oxford, 1998).

[72] F. Mouhat and F.-X. Coudart, Necessary and sufficient elastic stability conditions in various crystal systems, Phys. Rev. B **90**, 224104 (2014).

[73] S. F. Pugh, Relations between the elastic moduli and the plastic properties of polycrystalline pure metals, Philos. Mag **45**, 823 (1954).

[74] R. Sanjines, M. Benkahoul, C. S. Sandu, P. E. Schmid, and F. Levy, Electronic states and physical properties of hexagonal β-Nb_2N and δ'-NbN nitrides, Thin Solid Films **494**, 190 (2006).

[75] Z. Qi, Z. Wu, D. Zhang, J. Zuo, and Z. Wang, Microstructure, mechanical properties and oxidation behaviors of magnetron sputtered NbN_x coatings, J. Alloys Compd. **675**, 22 (2016).

[76] G. Y. Guo, S. Murakami, T.-W. Chen, and N. Nagaosa, Intrinsic Spin Hall Effect in Platinum: First-Principles Calculations, Phys. Rev. Lett. **100**, 096401 (2008).

[77] T.-Y. Hsieh, B. B. Prasad, and G. Y. Guo, Helicity-tunable spin Hall and spin Nernst effects in unconventional chiral fermion semimetals XY (X = Co, Rh; Y = Si, Ge), Phys. Rev. B **106**, 165102 (2022).

[78] G. Y. Guo, Anisotropic spin Hall and spin Nernst effects in bismuth semimetal, J. Magn. Magn. Mater. **563**, 169949 (2022).

[79] C. Kittel, *Introduction to Solid State Physics*, 8th ed. (Wiley, Hoboken, NJ, 2005).

[80] A. Sommerfeld, Zur Elektronentheorie der Metalle auf Grund der Fermischen Statistik, Z. Phys. **47**, 1 (1928).

[81] P. Ravindran, L. Fast, P. A. Korzhavyi, B. Johansson, J. Wills, and O. Erikkson, Density functional theory for calculation of elastic properties of orthorhombic crystals: Application to $TiSi_2$, J. App. Phys. **84**, 4891 (1998).